Journal of the European Ceramic Society **15** (1995) 537–549

0955-2219/95/$9.50

0955-2219(95)00010-0

Experimental Study of the Ti–B–C System Using LPCVD

M. A. Guiban* & G. Malé†

Laboratoire de Science et de Génie des Matériaux et des Procédés du C.N.R.S., BP 5, Odeillo, 66125 Font-Romeu Cedex, France

(Received 29 September 1994; revised manuscript received 6 December 1994; accepted 12 December 1994)

Abstract

The chemical system Ti–B–C–Cl–H was explored experimentally under reduced pressure (10 mbar) starting from a mixture of $TiCl_4$, BCl_3, CH_4 and H_2. The rate of growth, the composition, and the microstructure of the deposited solids were examined. The formation of titanium diboride, present in the entire explored domain, directs the chemical system. Carbon is present only in a small domain and when the concentration of $TiCl_4$ in the gas mixture is very low. Only rhombohedral boron carbide $B_{13}C_2$ and a tetragonal phase noted 'Q' with the general formula $B_{48}Ti_{2-x}C_{2-y}$ were identified, and always in the presence of TiB_2. These solids are distinguished by their very unique and varied microstructures and with the notable existence of nanometric three phase composites.

1 Introduction

The results presented, can be added to other research trying to improve certain properties of boron carbides by adding a third element to the basic boron–carbon system. A small improvement in its reactivity at a high temperature was made using silicon.[1] In this study, titanium was added to the system to evaluate its action on the mechanical properties.

In the domain of high performance ceramic materials, the Ti–B–C system is important because one can hope to obtain *a priori* the main compounds: $B_{13}C_2$, TiC and TiB_2 and their associated characteristics. The system was studied using chemical deposition starting from the gas phase under reduced pressure (LPCVD), which follows the study of the deposition, at thermodynamic equilibrium, of the solid phases starting with mixtures $TiCl_4$, BCL_3, CH_4 and H_2.[2]

It appears that the system is mainly controlled by the strong affinity between titanium and boron. The diagram in Fig. 1 shows that the concentration of $TiCl_4$ strongly influences the nature of the condensed phases and extends their domain boundaries. By contrast, the effect of the CH_4 concentration is minimal and it acts principally on the size deposition domain of the free carbon.

From these results and those of the other authors also cited in Ref. 2, it was determined that the prevailing compound in the system is TiB_2 and that combinations between the carbides of titanium and of boron, although *a priori* interesting, are not thermodynamically possible. Nevertheless, the possibility of codepositing titanium diboride and boron carbide in a narrow region exists.

2 Experimental Methods

The experiments were carried out in a CVD cold wall reactor. The substrates, heated by high frequency induction, are graphite cylinders 16 mm in diameter, and 5 mm high.

$TiCl_4$ titanium precursor, is mixed with the typical reactants used for studying the boron–carbon system (BCl_3, CH_4, and H_2). Being a liquid at ambient temperatures, its vapor is entrained by bubbling hydrogen. The considered parameters are the total pressure in the reactor (P), the temperature of the substrate (T) and the flow rate of the reactants (DX).

For practical reasons, the amount of boron trichloride (D BCl_3) was fixed. This allows one to consider the parameter $R = 100D\ CH_4/(D\ CH_4 + D\ BCl_3)$, representing the variation in the methane flow. Additionally the quantity of $TiCl_4$ participating in the reaction is controlled by the fraction of the flow rate of hydrogen carrying $TiCl_4$.

The characterization of the deposited solids depends on the following:

*New address: Sollac, rue du Compte Jean, Grande-Synthe, BP 2508, 59381 Dunkerque Cedex 1, France
†To whom correspondence should be addressed.

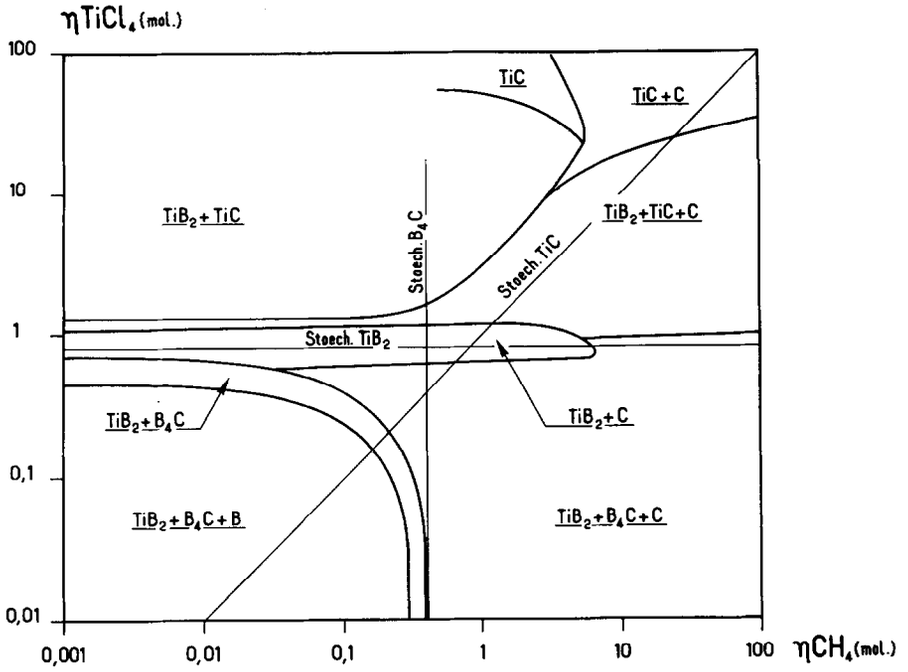

Fig. 1. Theoretical deposition diagram as a function of the gas phase composition.[2] T = 1300 K, P = 10 mbar, n BCl_3 = 1·6 mol, n H_2 = 15 mol.

The determination of the rate of deposit (gain of mass of the substrate per unit time).
The identification of the species by X-ray Difraction (XRD).
The elemental analysis by Electron Microprobe (EM).
The observation of morphology of the surface by Scanning Electron Microscopy (SEM).

3 Influence of the Composition of the Gas Mixture

The initial experiments principally involved control of the concentration of the reactants in the gas phase by varying the flows of $TiCl_4$ and CH_4.

The experimental parameters were the following:

T = 1300 K, P = 10 mbar, D H_2 = 15 lh^{-1}, D BCl_3 = 1·6 lh^{-1}
0·177 < D CH_4 < 9 lh^{-1} is $10^{-2} < D\ CH_4/D_T < 0{\cdot}35$
0·01 < D $TiCl_4$ < 0·4 lh^{-1} is $4 \times 10^{-4} < D\ TiCl_4/D_T < 2{\cdot}4 \times 10^{-2}$
D_T = Total flow

3.1 Identification of the phases

An XRD analysis of the solid deposits obtained from the experiments indicated three phases: titanium diboride (TiB_2), a rhombohedral $B_{13}C_2$ solid solution and a tetragonal phase that we labeled Q, which is of the same type as the phase $B_{50}C_2$ obtained in the B–C system.[3]

The distribution of these phases and their domains are shown in the deposition diagram of Fig. 2,

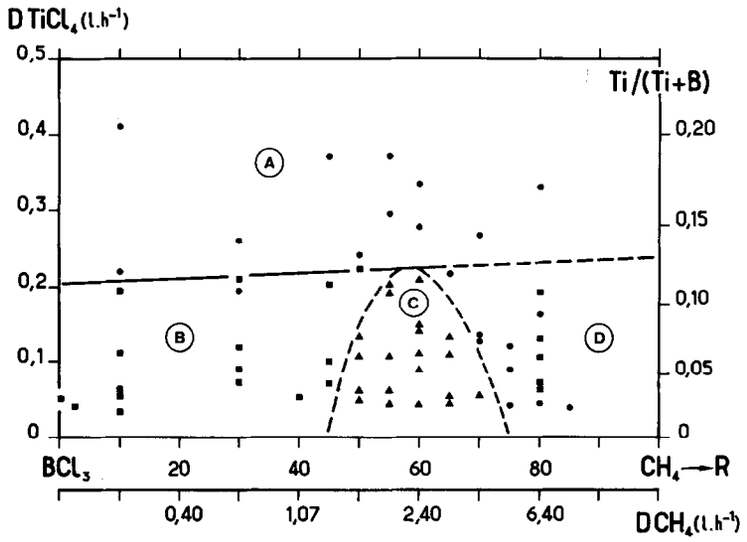

Fig. 2. Experimental deposition diagram as a function of the gas phase composition (XRD). T = 1300 K, P = 10 mbar, D BCl_3 = 1·6 lh^{-1}, D H_2 = 15 lh^{-1}. (A) TiB_2; (B) TiB_2 + Q; (C) $B_{13}C_2$ + TiB_2 + Q; (D) TiB_2 + Q.

which delineates four distinct zones: Zone A: Only TiB_2 is detected for flows of $TiCl_4$ greater than 0·2 lh^{-1} regardless of the value of *R*. For flows below 0·2 lh^{-1}, the phases $B_{13}C_2$ and Q appear. Zone B: The co-deposition of TiB_2 + phase Q is obtained for a ratio *R* less than 45. The proportion of the tetragonal phase in the mixture is more important since the two variables are lower. Zone C: The two compounds $B_{13}C_2$ and TiB_2 and the tetragonal phase Q are deposited simultaneously for values of *R* between 45 and 75. This domain becomes narrower when the flow of $TiCl_4$ is augmented. Zone D: As in Zone B, the TiB_2 and tetragonal phase coexist. Phase Q is present in a very small quantity, and is not always detected by XRD.

In agreement with the thermodynamic predictions,[2] the compound TiB_2 was synthesized in all the explored parametric domain. However, its crystallization in the depositions considered to be monophased is much better, as the gaseous mixture has a low concentration of methane and is rich in $TiCl_4$ (Fig. 3). Indeed an evolution towards the conventional conditions for the production of TiB_2, in which the ratio Ti/B in the gaseous phase is close to that in the condensed phase.

The carbonaceous phases appear jointly with TiB_2 but only for low concentrations of $TiCl_4$ in the gaseous phase. The most frequently encountered phase is the tetragonal (Q) one, probably not containing much carbon.

In fact, this phase clearly has phases very rich in boron such as $B_{50}C_2$, $Ti_{1\cdot87}B_{50}$ or $Ti_{1\cdot3\text{-}2}B_{48}C_2$ as described by Amberger and Ploog.[5–8] Figure 4 compares the RX spectra of the experimental phase Q to those of $B_{50}C_2$, $Ti_{1\cdot87}B_{50}$ or $Ti_{1\cdot86}B_{48}C_2$.

The configuration of the spectrum of the Q phase is identified with that proposed by Amberger, as much by the sequence of the peaks as by their position. The relative intensities of the peaks, by contrast, are not as reported, but the variation can be attributed to the textural effects of our material. In addition, some peaks were found which are not listed in the JCPDS data (no. 29-1356). However, a theoretical calculation of their position based on the lattice parameters determined (Table 1), allowed us to attribute these additional peaks to the tetragonal phase.

During prolonged reheating at 1670 K, this phase dissociated completely, forming $B_{13}C_2$ (the only additional phase detected), but probably also TiB_2 (already present), and boron (not detected because the amounts present are too small).

the spectra of the deposited two and three phases (Fig. 5) show that the proportion of the tetragonal phase decreases rapidly when the flow of $TiCl_4$ increases. Additionally, they show that the XRD peaks relative to the most carbonaceous phase of the system, rhombohedral boron carbide ($B_{13}C_2$), are less numerous, less intense and poorly defined.

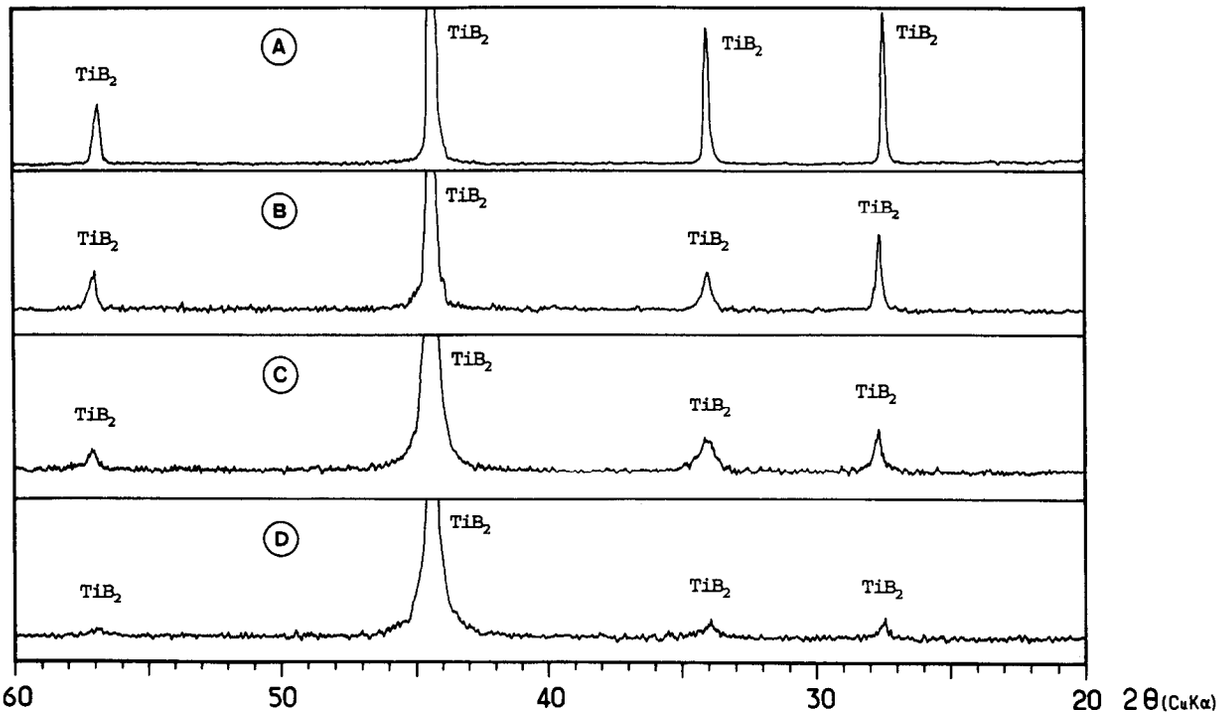

Fig. 3. States of titanium diboride crystallisation. T = 1300 K, P = 10 mbar, D BCl_3 = 1·6 lh^{-1}, D H_2 = 15 lh^{-1}

	A	B	C	D
R	10	55	70	80
D $TiCl_4$ (lh^{-1})	0·40	0·29	0·27	0·16

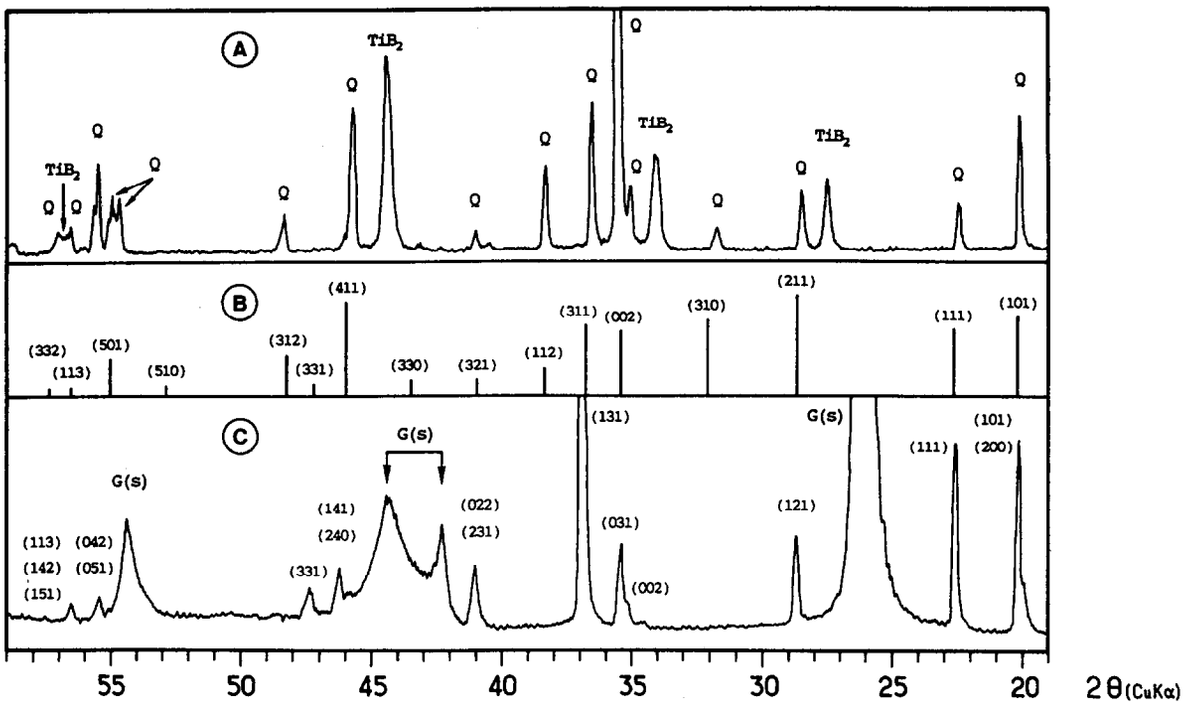

Fig. 4. Identification of the tetragonal phase (Q). (A) RX Spectrum of the B deposition domain (TiB_2 + Q); (B) Theoretical RX Spectrum of $B_{50}Ti_{1\cdot87}$;[6] (C) RX Spectrum of the $B_{50}C_2$ phase (G(s): graphite substrate).

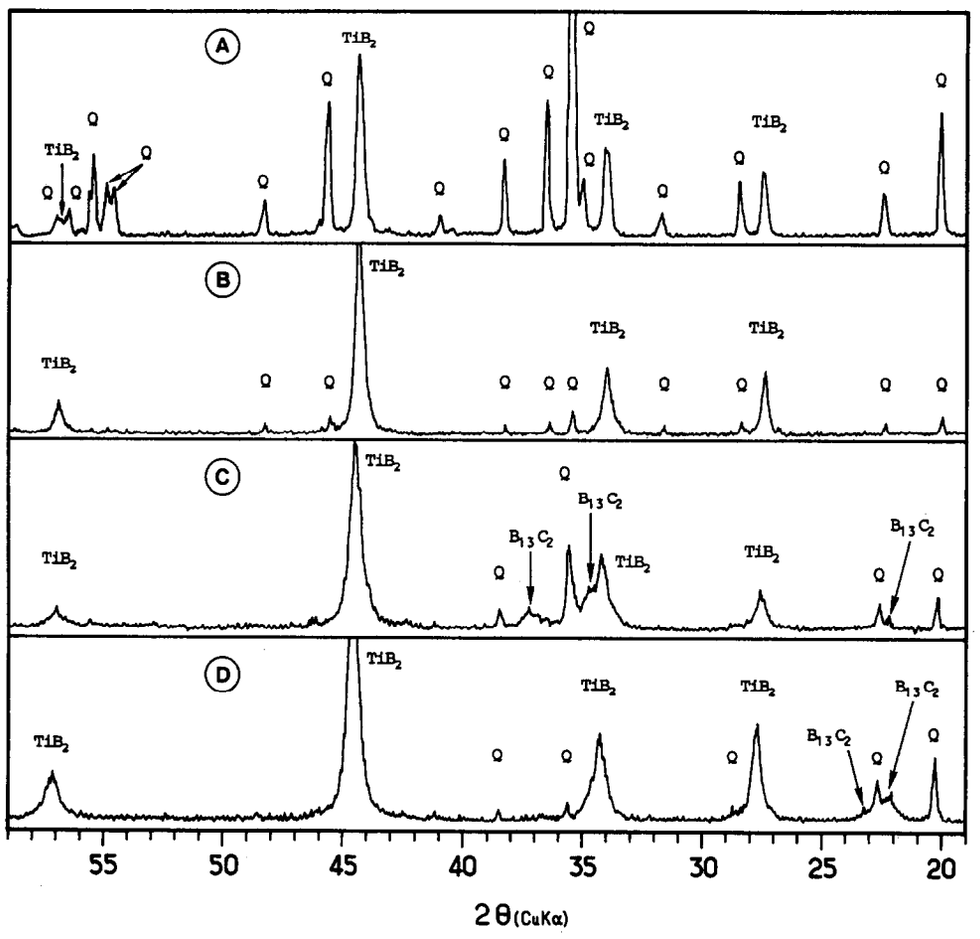

Fig. 5. Evolution of the RX spectra of the two or three phase depositions as a function of the composition in the gas phase:

	A	B	C	D
R	10	10	50	70
D $TiCl_4$ (lh^{-1})	0·014	0·10	0·06	0·054

Table 1. Lattice parameters of the main tetragonal phases

Phase	*a(A)*	*c(A)*	*Reference*
$B_{50}C_2$	8·77	5·07	[5]
$Ti_{1·87}B_{50}$	8·830	5·072	[6]
$Ti_{1·86}B_{48}C_2$	8·870	5·062	[7,8]
Q	8·84 ± 0·01	5·05 ± 0·01	

3.2 Elemental Analysis

Sixteen of the deposited phases distributed throughout the domains of the phase diagram (Fig. 6) were analysed using an electronic microprobe on polished sections. The results of the elementary bulk (defocalization of the electronic beam on a 20 μm diameter) and local analyses on the different visualized phases are averaged from 5 to 10 measurements. The results are grouped in Table 2 and show that the deposits are of a heterogeneous composition at the level of the analysis.

The global compositions are very rich in boron and are found in only a small part of the ternary Ti–B–C diagram. Three types of composition are observed among the local analyses:

(1) The first type corresponds to TiB_2; several percent of carbon are always associated with it.

(2) The second type (92–95 atomic percent boron, 4·5 to 5·5 atomic percent titanium, and 0·5–3 atomic percent carbon) is identified with the tetragonal structure $Ti_{1·3-2}B_{48}C_2$ such that the titanium content is slightly higher and the carbon content is slightly lower as compared to the domain of the solution proposed by Amberger.[8]

(3) The third type of compound which logically corresponds to the $B_{13}C_2$ phase observed by XRD, introduces some important quantities of titanium (from 7–26 atomic percent).

This third composition could be considered as a mixture of the three phases, TiB_2, Q, and $B_{13}C_2$ identified by XRD and forming a dispersed type of material (hereafter designated 'M') for which the size of the crystals would be inferior to the resolution for the spot of analysis.

A deposition diagram was outlined from these analyses (Fig. 7). In this diagram, at the most only two of the three types of the previously defined compositions coexist. The boundary of the monophased zone of the deposition TiB_2 is shifted toward higher flows of the $TiCl_4$ (around 0·3 lh^{-1} as compared with 0·2 lh^{-1} previously). Below this value, the dispersed phase 'M' is always present, either alone or associated with the phases TiB_2 or Q.

3.3 Rate of growth of the coatings

The deposition rates are expressed in units of mass per unit time and area, where the changes in mass were determined by weighing the samples before and after applying the coating.

3.3.1 Effects of varying methane concentration of the deposition rate

Figure 8 shows that for a constant flow of $TiCl_4$, the deposition rate varies little with the methane flow for values of R between 45 and 60, following the flow of $TiCl_4$. For higher values, the deposition rate decreases. This evolution could correspond to the progressive disappearance in the deposited solids of the large crystals of TiB_2 or the Q phase for which the kinetics of growth are elevated. The rate decreases in the zones of the phase diagram where only the dispersed phase 'M' is found.

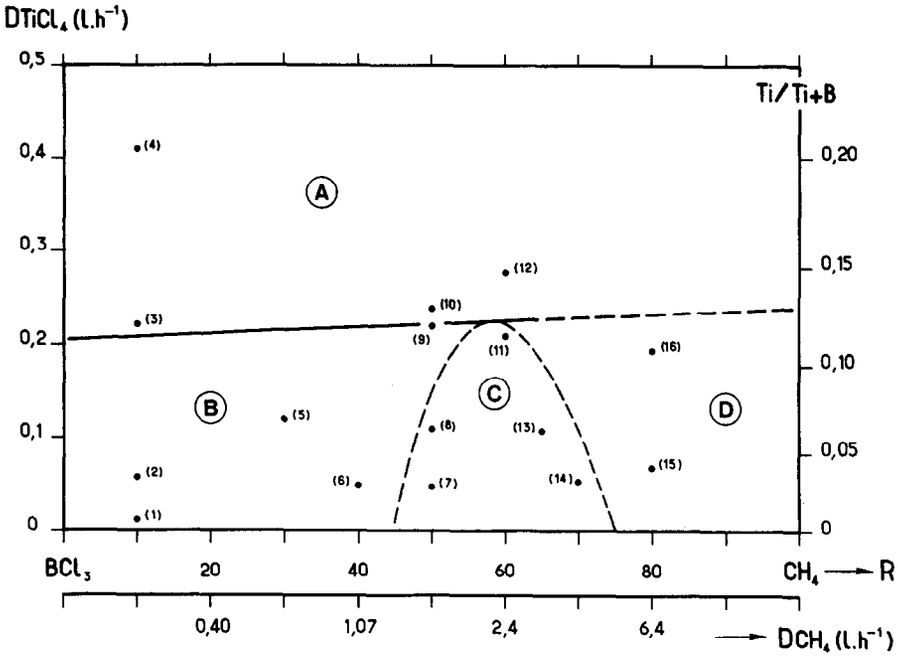

Fig. 6. Position of the analysed samples (electronic microprobe).

Table 2. Elemental analysis of layers

Sample	Bulk analyses (at.%)			Local analyses (at.%)								
				TiB_2			Q			'M'		
	B	Ti	C	B	Ti	C	B	Ti	C	B	Ti	C
1	90·0 ± 2	5·8 ± 1	4·2 ± 1				94·0 ± 2	4·5 ± 0·5	1·5 ± 4	80·0 ± 4	12·0 ± 1	7·0 ± 0·5
2	87·2 ± 3	11·2 ± 1·5	1·6 ± 0·5				95·0 ± 1	4·5 ± 1	0·5 ± 0·5	74·0 ± 3	23·0 ± 1	3·0 ± 0·5
3	78·8 ± 3	18·9 ± 1	2·3 ± 0·5				92·6 ± 3	5·4 ± 1	2·0 ± 0·5	74·0 ± 1	24·0 ± 1	2·0 ± 0·5
4	71·0 ± 3	26·8 ± 2	2·2 ± 0·5	66·0 ± 1	33·0 ± 0·5	1·0 ± 0·5						
5	85·7 ± 4	12·3 ± 0·5	2·0 ± 0·5				93·3 ± 2	4·9 ± 0·5	1·8 ± 0·5	78·6 ± 4	19·4 ± 0·5	2·0 ± 0·5
6	85·3 ± 4	10·3 ± 1·5	4·3 ± 0·5				93·0 ± 1	4·0 ± 0·5	3·0 ± 0·5	80·0 ± 2	17·0 ± 1	3·0 ± 0·5
7	84·3 ± 2	7·0 ± 2	8·7 ± 1							84·3 ± 1	7·0 ± 1	8·7 ± 0·5
8	81·2 ± 4	14·0 ± 2·5	4·8 ± 1							81·5 ± 4	13·5 ± 2·5	5·0 ± 1
9	71·2 ± 5	26·5 ± 1·5	2·3 ± 0·5							71·2 ± 5	26·5 ± 1·5	2·3 ± 0·5
10	75·2 ± 5	17·8 ± 2	7·1 ± 0·5	67·0 ± 1	30·0 ± 0·5	3·0 ± 0·5				72·0 ± 2	21·0 ± 0·5	6·0 ± 0·5
11	72·2 ± 5	21·2 ± 5	6·6 ± 1	64·5 ± 2	34·0 ± 0·5	1·5 ± 0·5				73·0 ± 2	23·0 ± 1	4·0 ± 0·5
12	69·0 ± 2	29·3 ± 1	1·7 ± 0·5	67·6 ± 2	29·4 ± 1	2·2 ± 0·5						
13	78·5 ± 7	16·0 ± 5	5·5 ± 1							76·5 ± 7	19·0 ± 0·5	4·5 ± 1
14	81·2 ± 2	10·9 ± 1	7·9 ± 0·5							81·2 ± 2	10·9 ± 1	7·9 ± 0·5
15	78·9 ± 2	11·3 ± 2	9·8 ± 1							78·9 ± 2	11·3 ± 2	9·8 ± 1
16	69·1 ± 8	25·5 ± 3	5·4 ± 1·5	66·0 ± 2	32·0 ± 1	2·0 ± 0·5				72·0 ± 2	21·0 ± 1	7·0 ± 0·5

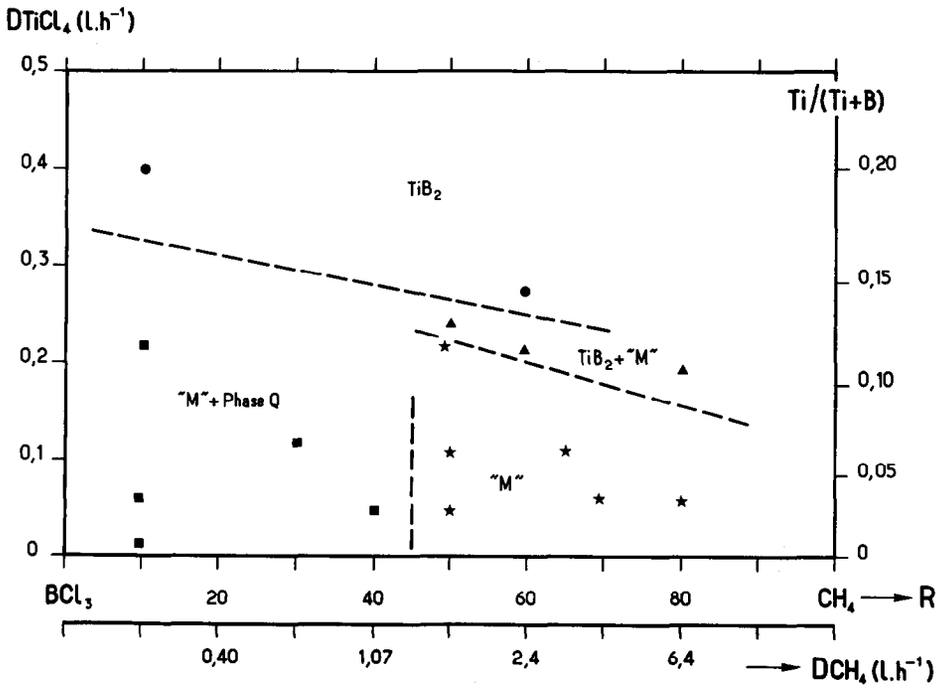

Fig. 7. Diagram of the deposition based an elemental analysis 'M': TiB_2 + $B_{13}C_2$ + Q.

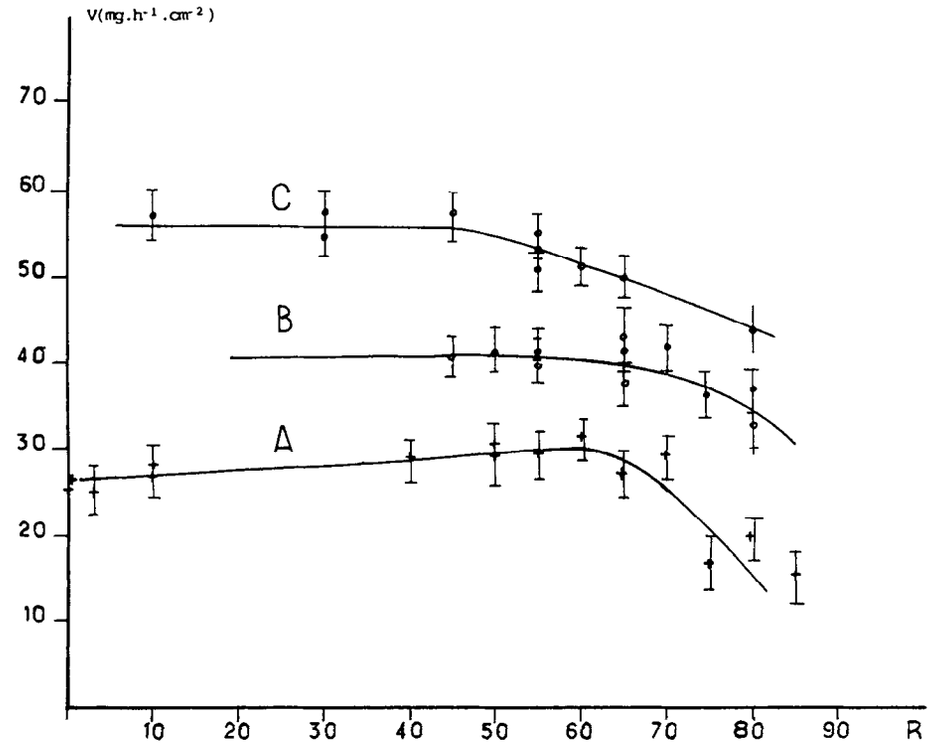

Fig. 8. Evolution of the deposition rate as a function of the methane concentration (R). T = 1300 K, P = 10 mbar, D BCl_3 = 1·6 lh^{-1}, D H_2 = 15 lh^{-1}. (A) D $TiCl_4$ = 0·05 lh^{-1}; (B) D $TiCl_4$ = 0·12 lh^{-1}; (C) D $TiCl_4$ = 0·21 lh^{-1}.

3.3.2 Effects of varying $TiCl_4$ concentration on the deposition rate

The influence of the $TiCl_4$ flow is clearly stronger. The rate of deposition increases rapidly with the flow of titanium tetrachloride. For example, the rate doubles when the flow increases from 0·05 to 0·2 lh^{-1}. The curve in Fig. 9(a) gathers the values obtained for values of R less than 60, which is in the domain where the concentration of CH_4 doesn't have any influence. A maximum rate is obtained for flows of $TiCl_4$ on the order of 0·2–0·25 lh^{-1}.

An analog result was established by Takahashi *et al.*[9] for the system $TiCl_4$–BCl_3–H_2 (Fig. 9(b)), giving evidence of the importance of the formation of diboride in the kinetics of the deposition.

3.4 Microstructure of the deposited layers

The crystallization of the solid phase varies strongly as a function of the composition of the gaseous mixture provoking in particular some unique surface morphologies.

3.4.1 Morphology of the surface

(a) Low flows of $TiCl_4$

If the concentration of the CH_4 is also low, the coatings are rich in the tetragonal phase. The phase $B_{50}C_2$ in the B–C system[4] is present as angular crystals of a large size (up to about 30 μm), but for which the geometry is seldom perfect (Fig. 10(a)). When the flow of methane increases, the crystallization becomes finer, and the growth becomes dendritic. Meanwhile, the concentration of angular crystals in the tetragonal phase decreases sharply and their size is clearly smaller (a few μm).

Near R = 50 (Fig. 9(b)), the surface shows some growth of the order of 10 μm and of a rounded form, characteristic of a mixture with a boron carbide base ('M') when this is the main phase present.

For greater methane flows, the growth increases (~100 μm) (Fig. 9(c), R = 65). Beyond the three phases domain (XRD), the small sub-micronic crystals are very well defined geometrically and are already formed (Fig 9(d), R = 80).

(b) Influence of the $TiCl_4$ flow

When the flow of $TiCl_4$ increases, the titanium diboride has the general tendency to form in large quantities and to become the basic material in the deposition.

In this matrix, with a low flow of methane, the crystals in the tetragonal phase are small in size (a few microns) and become more scattered as the $TiCl_4$ concentration in the gaseous mixture increases. Near R = 60 (Fig. 10(e)) the growths visible at the surface become less and less numerous, and consist of the 'M' mixture.

At high methane concentrations (R > 65) and for a $TiCl_4$ flow on the order of 0·25 lh^{-1}, the surface shows, under small magnification, aspects of an amorphous material. It is in fact comprised of the small crystals remarkably uniform and of a few μm in size (Fig. 10(f)).

3.4.2 Examination of transversal cuts

On the plates shown in Fig. 11, obtained from

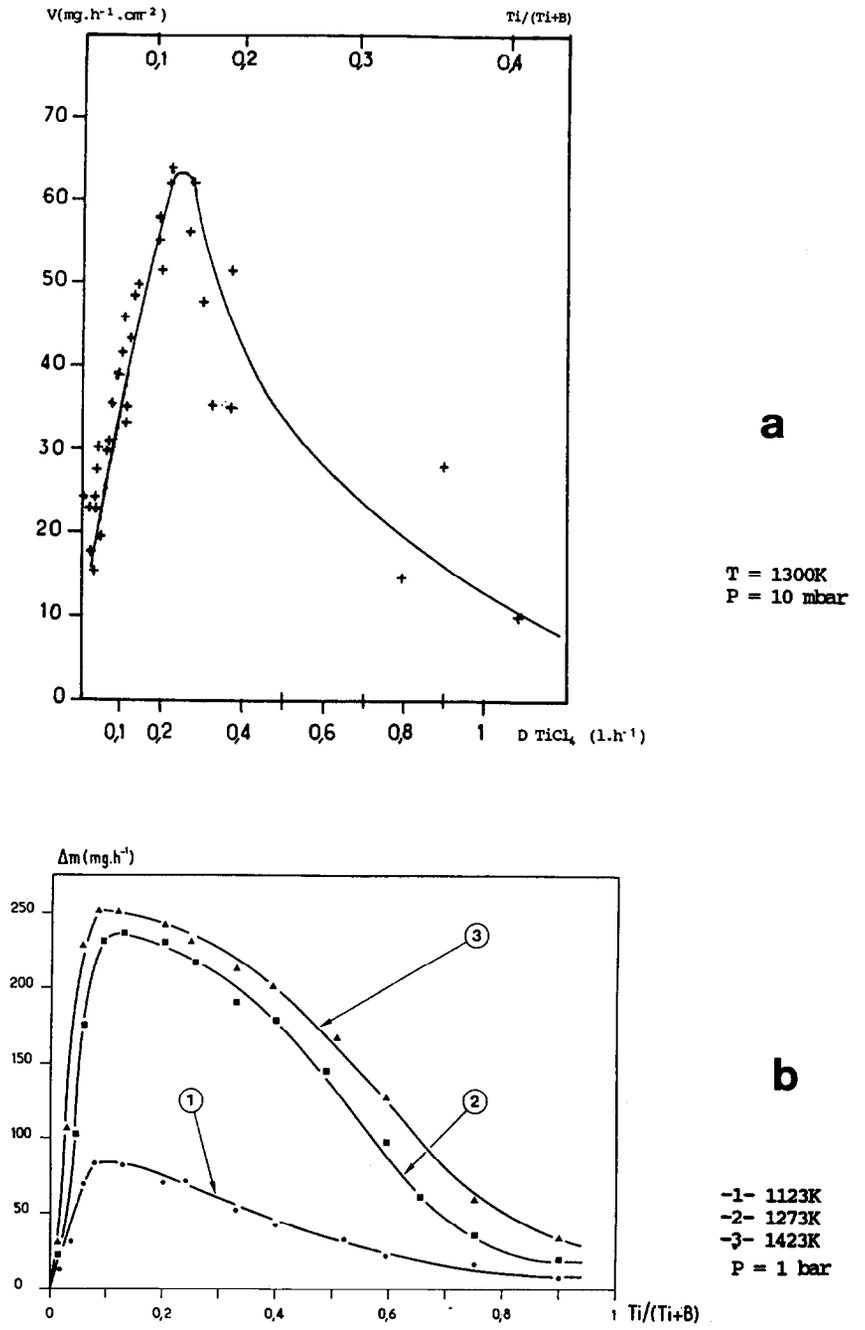

Fig. 9. Influence of the $TiCl_4$ concentration on the deposition rate $R<60$. (a) T = 1300 K, P = 10 mbar, D BCl_3 = 1·6 lh^{-1}, D H_2 = 15 lh^{-1}; (b) Influence according to Takahashi[9] (Ti–B system).

backscattering electrons, the microstructure can be seen clearly: the rich titanium (TiB_2) zones appear clearly and contrast strongly with the shadowed low titanium regions (Q and $B_{13}C_2$). The materials in the 'M' + Q domain are very dense. When the tetragonal phase is preponderant (Fig. 11(a)), the crystals grow perpendicularly to the surface. When it becomes less abundant, the orientation is uncertain (Fig. 11(b)). In the domain 'M', the crystallization is particular. The tetragonal phase is always present in a matrix formed from a mixture of boron carbide and titanium diboride (B_4C + TiB_2), either in the form of filaments without defined geometry (Fig. 11(c)) or under the form of the axis of the grain (Fig 11(d)).

The composition of the matrix is not constant. Near the interface of the substrate and deposition as well as at the center of the nucleation site, the titanium content is higher. When the size of the particles is large, this type of growth leads to the formation of large pores.

The matrix appears homogeneous with the electronic microprobe analysis. The resolution was obtained by field effect microscopy (Fig. 12(a) and 12(b)). It shows that the matrix is constituted of a dispersed mixture of nanometric crystals (about 50 nm) of a boron carbide and titanium diboride ($B_{13}C_2$ + TiB_2). The grains formed here are often found following an axis parallel to the surface with whiskers of phase Q and a cross section of about

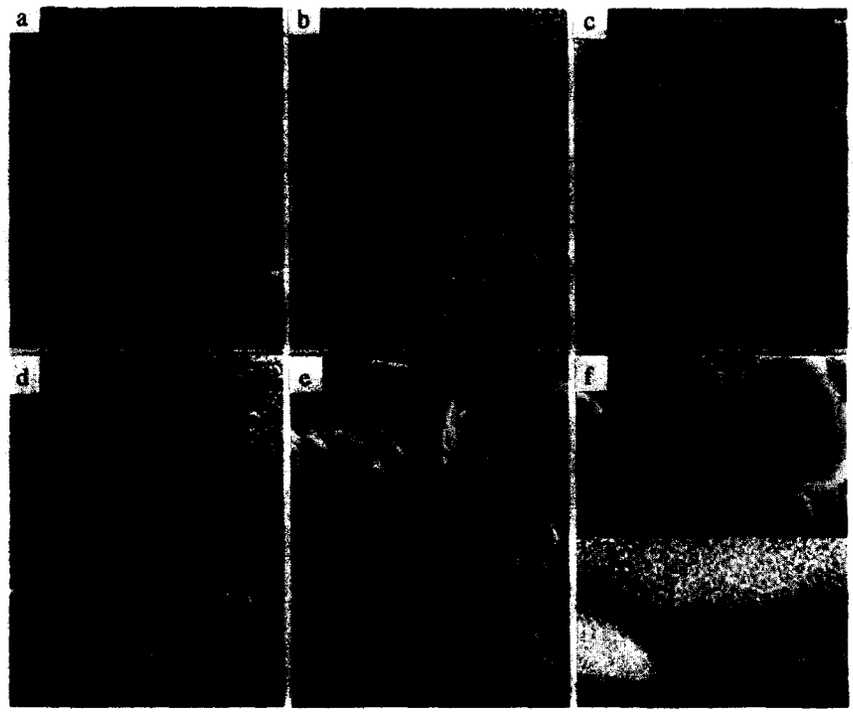

Fig. 10. Morphology of typical deposition surfaces. T = 1300 K, P = 10 mbar, D BCl_3 = 1·6 lh^{-1}, D H_2 = 15 lh^{-1}. (a) Q + 'M' (R = 10); (b) 'M' (R = 50); (c) 'M' (R = 65); (d) 'M' (R = 80); (e) TiB_2 + 'M' (R = 60); (f) TiB_2 + 'M' (R > 65).

0·5 × 0·5 μm. In the domain TiB_2 + 'M', the depositions form over a wide area and have very fine microstructure (Fig. 11(e)). The compounds evolve from 'M' to TiB_2 in forming some zones parallel to the surface. The concentration of TiB_2 is always higher near the interface. The deposits of pure TiB_2 (Fig. 11(f)) equally present a layered structure with very porous periodic layers and are characteristic of those described by Takahashi.[9] These TiB_2 coatings were obtained with weak ratios of Ti/Ti+B.

4 Influence of the Temperature

4.1 Kinetics and the nature of the phases

The results of the experiments with R = 60 and the $TiCl_4$ flow equal to 0·015 lh^{-1}, are shown in Fig. 13(a). At temperatures above 1530 K, the tetragonal phase, which is unstable at high temperatures no longer forms and a codeposit of titanium diboride and boron carbide is found. In contrast, at temperatures below 1280 K, titanium boride is the only phase identified.

The corresponding rate of deposition increases with temperature until 1500 K and then falls quickly at temperatures greater than about 1600 K. This rapid rate decrease can be attributed to the appearance of reactions in the homogenous phase. This tendency was established for the B–C system at the same ratio R.[10,11]. By contrast, the work of Besmann[12] indicates that the TiB_2 deposition rate continues to increase until 2173 K but this increase is lowered as soon as the temperature reaches 1473 K. Thus, the addition of methane essentially limits the deposition rates at high temperatures.

This effect was confirmed when the methane flow was decreased (R = 10, D $TiCl_4$ = 0·05 lh^{-1}). The deposition rate, which was higher than earlier, increased linearly with temperature (Fig. 13(b)). The tetragonal phase was observed up to our highest experimental temperature of 1580 K.

Figure 14(a) shows the deposition rate as a function of temperature for two $TiCl_4$ flow rates. In this case, the flow of BCl_3 was reduced to 0·4 lh^{-1} in order to decrease the kinetics, and R was fixed at 60. The evolution is the same as was described previously (Fig. 13(a)), but an increase in the $TiCl_4$ gas phase concentration displaces the maximum value towards lower temperatures and since the concentration of CH_4 is less, it has a smaller influence on the rate decrease. Figure 14(b) outlines the corresponding deposition diagram. The existence of the two phase region (TiB_2 + Q and TiB_2 + $B_{13}C_2$) and the three phase region (TiB_2 + B_{13} C_2 + Q) appears to be strongly dependent on temperature.

Furthermore, as was mentioned earlier, the carbon phase exist only when $TiCl_4$ concentrations are small. In this case, for flows of $TiCl_4$ > 0·1 lh^{-1}, only TiB_2, is found.

4.2 Surface morphology

The surface morphology, like the composition of the deposits, varies greatly with temperature. For

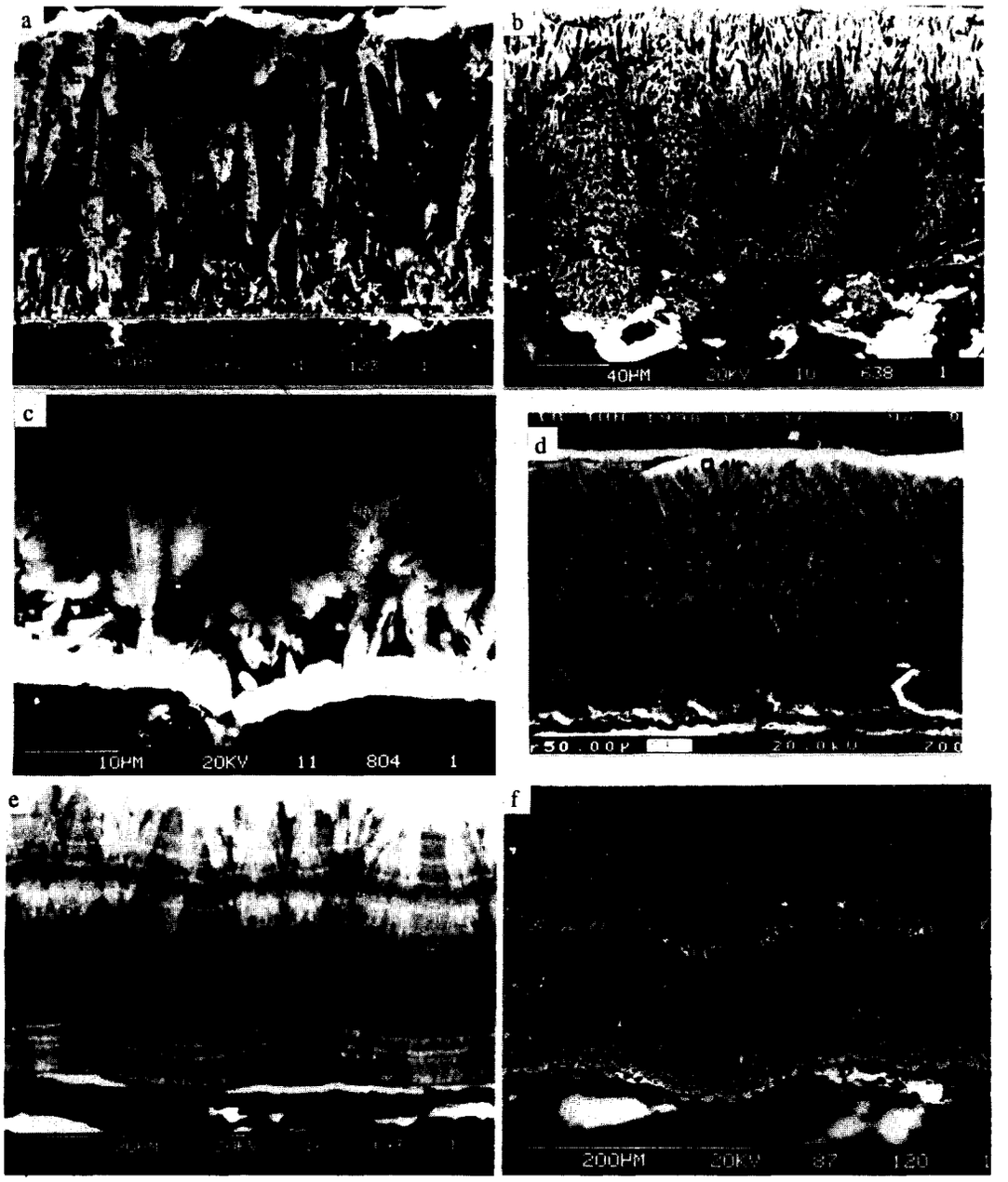

Fig. 11. Metallographic sections of typical deposits (secondary electrons). (a) and (b) 'M' + Q; (c) and (d) 'M'; (e) TiB_2 + 'M', (f) TiB_2.

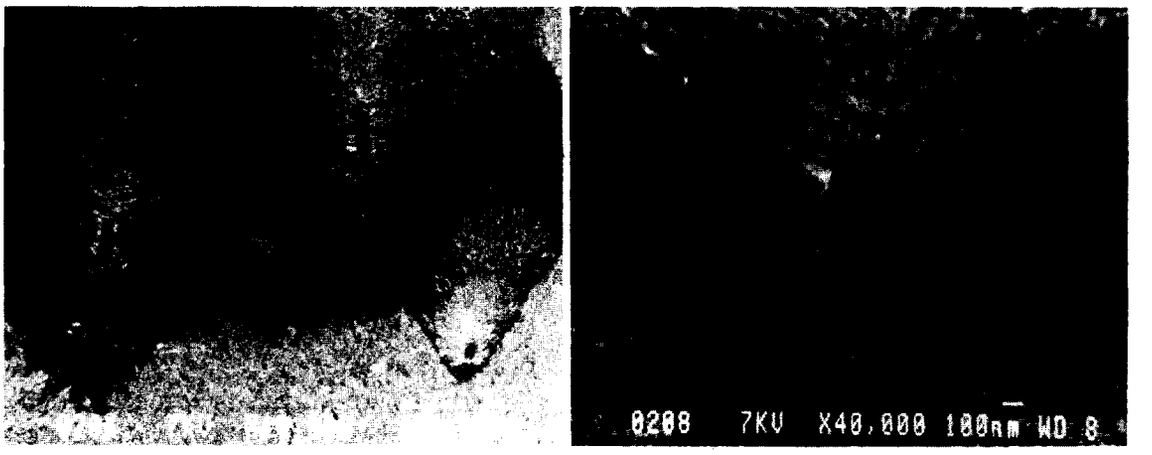

Fig. 12. Microstructural details of a type 'M' deposition (field effect microscopy). R = 65, D $TiCl_4$ = 0·108 lh^{-1}.

R = 60 and D $TiCl_4$ = 0·06 lh^{-1} and at low temperatures (only TiB_2 deposition), the surface has the characteristic partial crystallization (Fig. 15(a)). When the temperature is elevated, the tetragonal phase, which has a tendency to grow in a columnar manner, greatly influences the microstructure

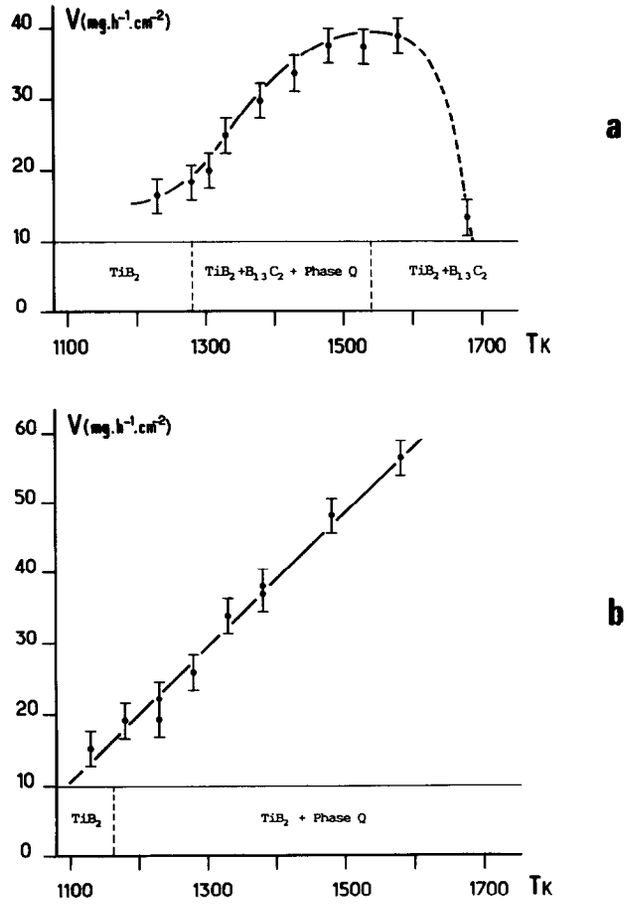

Fig. 13. Influence of the temperature on the deposited phases and on the deposition rate. P = 10 mbar, D BCl_3 = 1·6 lh^{-1}, D H_2 = 15 lh^{-1}. (a) R = 60; D $TiCl_4$ = 0·015 lh^{-1}; (b) R = 10, D $TiCl_4$ = 0·05 lh^{-1}.

of the layers. In particular, a reduction of its content is accompanied by progressive disorientation of the emerging crystals. At 1380 K for example, the surface is typical of a singular crystallization in the previously described 'M' phase (Fig. 15(b)).

Beyond 1580 K, only TiB_2 is identified. This time its crystallization is clearly evident with XRD, but it can be present under a wide variety of morphologies: fine lamellar structure at 1580 K and parallelepipedal crystals at 1685 K (Figs 15(c) and (d)).

5 Conclusions and Comments

The results of this experimental study have little in common with the thermodynamic predictions previously published.[2] The only principal in agreement is the importance of the affinity of the boron and titanium to the behavior of the chemical system. This is evident in all the cases by the omnipresence of titanium diboride in the explored regions. By contrast, the carbon vector has a weak influence experimentally, and it is only for cases with low $TiCl_4$ concentrations in the initial gas mixture that the weakly carbonated phases (Q and $B_{13}C_2$) are deposited.

According to the theoretical results, methane should be almost completely dissociated and accordingly, carbon should be the major element in coatings prepared from a gaseous starting mixture rich in methane. But, neither titanium carbide nor free carbon were ever detected.

If we compare the theoretical deposition diagrams with the experimental ones (Figs. 1 and 2), the experimental region of the $B_{13}C_2$ phase is found largely displaced towards higher values of CH_4 concentrations than in the theoretical diagram (region TiB_2 + B_4C + C) which indicates that an excess of methane (about ten times greater than the amount predicted by thermodynamics) is necessary to form $B_{13}C_2$. Similarly, the limits of the boron carbide domain are found at values less than those predicted by thermodynamics for specific amounts of $TiCl_4$ in the gas phase (Ti/Ti+B < 0·35).

Concerning yields: if one considers that titanium boride is essentially the compound formed when the maximum deposition rate is attained (Figs. 2 and 8), the ratio Ti/B is then about 1 : 6 or a third of the diboride stoichiometry. In this case, 50–60% of the $TiCl_4$ in the gas mixture reacted to form TiB_2. Thus the maximum theoretical yield of 95% as indicated by thermodynamics is not obtained. The discrepancies between the thermodynamic and experimental results can mainly predict the existence of the tetragonal phase Q which could not have been taken into account in the calculations and which also influences the microstructure of the deposited solids. This phase is a new example of the metastable phase which can be obtained far from equilibrium by CVD. It can be identified with the phases described by Amberger and Ploog[7–8] $Ti_{1\cdot87}B_{50}$ and $Ti_{2-x}B_{48}C_2$.

Nevertheless, the huge influence of titanium chloride in comparison to methane on the composition of the solid as well as the results of the local analysis (weak carbon content in the region of the 'Q' phase (Table 2)) leads one to think that, especially in the cases low in methane, the Q phase is more saturated in titanium than in carbon and could be written as $B_{48}Ti_2C_{2-y}$. The more general formulation would be $B_{48}Ti_{2-x}C_{2-y}$.

In other respects, the existence of the carbonaceous phase is also strongly influenced by the synthesis temperature. Their domain of thermal existence is in fact relatively limited (from 1150 to around 1700 K under our experimental conditions). The boundaries evolve however with different parameters. When the tetragonal phase can no longer form (at temperatures less than 1600 K in our work), a codeposit of titanium diboride and boron carbide occurs, which is an interesting *a priori* mixture from the mechanical properties

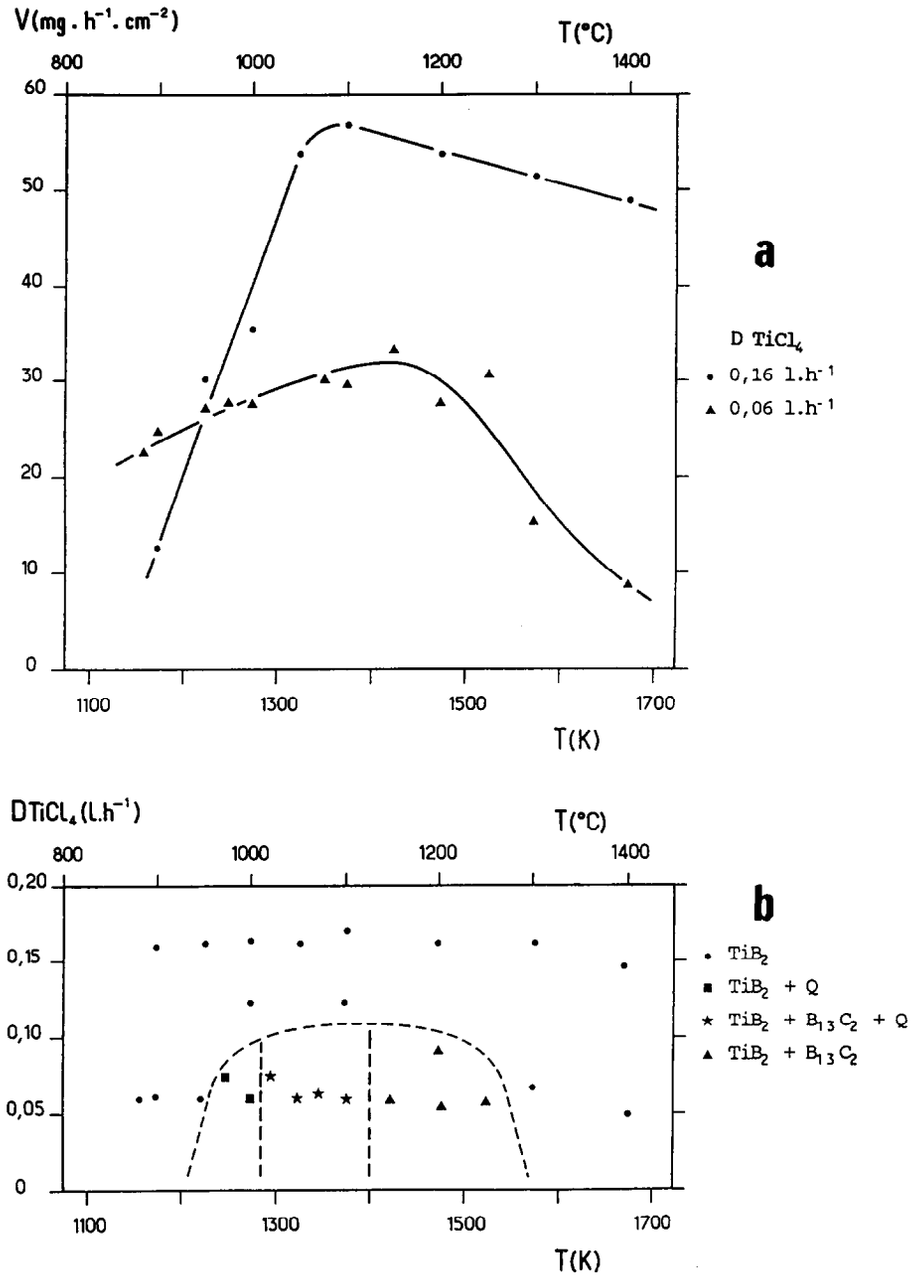

Fig. 14. Influence of temperature and of $TiCl_4$ concentration on the deposition rate (a) and on the nature of the deposited phases (b). P = 10 mbar, R = 60, D BCl_3 = 0·41 lh^{-1}.

stand-point. Since it makes $B_{50}C_2$ in the B–C–H–Cl system,[10,11] this tetragonal phase, very rich in boron, can strongly limit the deposition of non-combined boron at low temperatures. However, the phase obtained in this case differs from $B_{50}C_2$ by its large domain of existence (up to R = 80). Thus, it covers the entire deposition region of boron carbide, and the two phases TiB_2+$B_{13}C_2$ can only be isolated at higher temperatures. By contrast, the deposition domain of the rhombohedral phase is only slightly displaced or not displaced at all on the methane concentration axis as compared to the B–C–Cl–H system.

In conclusion, it can be observed that these carbonaceous phases, using a tridimensional representation of D CH_4 (R), D $TiCl_4$ and temperature, will only be present in a small zone within the large domain of TiB_2 deposition. In contrast, these phases are very interesting because of their very special and unique microstructure. The common basis of these materials is a mixture of nanometric crystals of titanium diboride and rhombohedral boron carbide which wrap the whiskers of phase Q and which also have different configurations. This composite, called 'M', can be mixed with diboride and the Q phase, which are present simultaneously in the same solid under two different crystallizations.

Acknowledgements

This research was supported by the Association Nationale de la Recherche Technique (A.N.R.T.)

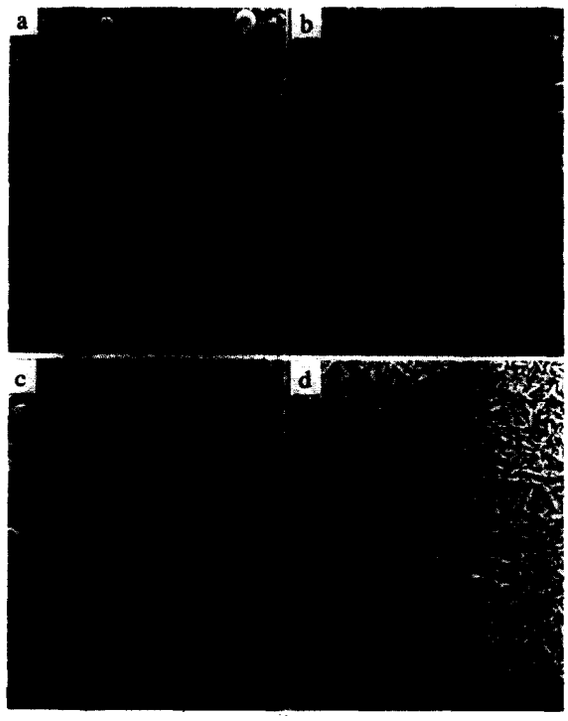

Fig. 15. Surface morphology as a function of temperature. P = 10 mbar, R = 60, D $TiCl_4$ = 0·06 lh^{-1}. (a) 1180 K; (b) 1380 K; (c) 1580 K; (d) 1685 K.

and by Coating Development S.A. (Ciffre convention no 86307).

References

1. Guiban, M. A., Berjoan, R. & Male G., *Ann. Chim. Fr.*, **18** (1993) 159–74.
2. Guiban, M. A. & Male, G., *Calphad*, **17**, 2 (1993) 207–16.
3. Guiban, M. A., Etude par CVD des systèmes Si–B–C–Cl–H et Ti–B–C–Cl–H. *Caractérisation des dépôts*, Thèse de Doctorat, Université de Limoges, 1991.
4. Lartigue, S. & Male G., *J. Mater. Science Letters*, **7** (1988) 153–6.
5. Ploog, K. & Amberger, J., *Less Common Met.*, **23** (1971) 33–42.
6. Amberger, E. & Polborn, K., *Acta Cryst.*, **B31** (1975) 949–53.
7. Ploog K., *Acta Cryst.*, **B32** (1976) 981–2.
8. Amberger, E. & Gerster, *Acta Cryst.*, **B36** (1980) 672–5.
9. Takahashi, T. & Kamia, H., *J. Cryst. Growth*, **26** (1974) 203–9.
10. Lartigue, S., *Elaboration par CVD et caractérisation de dépôts de carbure de bore. Application au revêtement de l'acier*, Thèse de Doctorat, Institut National Polytechnique de Grenoble, 1986.
11. Lartigue, S., Cazajous, D., Nadal, M. & Male, G., *Proc. Euro CVD 5*, Uppsala Sweden, June 17–20 1987 pp. 483–519.
12. Besman, M. & Spear, K. E., *J. Electrochem. Soc., Solid State Science and Technology*, **124**, 5 (1977) 790–7.